Thin Solid Films 811 (2025) 140611

Contents lists available at ScienceDirect

Thin Solid Films

journal homepage: www.elsevier.com/locate/tsf

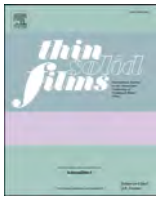

Dense Al_2O_3 films prepared by high power impulse magnetron sputtering at pulsed kV bias

Dongjie Yang [a,1], Yaoyao Liu [b,1], Xiang Zhang [a], Shusheng Chen [a], Xiaowei Wang [c], Yu Liao [a], Xiaokai An [a], Yanfei Zhao [b], Lingjie Chen [b], Suihan Cui [a,d], Liangliang Liu [a,d,*], Ricky K Y Fu [d], Paul K Chu [d], Zhongzhen Wu [a,*]

[a] School of Advanced Materials, Peking University Shenzhen Graduate School, Shenzhen 518055, PR China
[b] National Key Laboratory of Marine Corrosion and Protection, Luoyang Ship Material Research Institute, 471023, PR China
[c] Shenzhen Institute for Advanced Study, University of Electronic Science and Technology of China, Shenzhen, 518110, PR China
[d] Department of Physics, Department of Materials Science and Engineering, and Department of Biomedical Engineering, City University of Hong Kong, Tat Chee Avenue, Kowloon, Hong Kong, PR China

ARTICLE INFO

Keywords:
Alumina films
Film density
Kilovolt pulsed bias
High power impulse magnetron sputtering

ABSTRACT

Al_2O_3 films are often used in electronic and other devices for surface protection due to their excellent insulating and mechanical properties, but these properties depend on the film density. Conventional magnetron sputtering used industrially to deposit Al_2O_3 films faces challenges in density regulation, and many Al_2O_3 coatings have poor densities. Herein, negative kV biases are applied to the substrate in high-power impulse magnetron sputtering (HiPIMS) to produce the desirable high-energy ions to densify the Al_2O_3 films. Our results indicate that the high pulsed bias also mitigates arcing during the deposition of insulating alumina films. By increasing the pulsed voltage, the film density increases, resulting in higher optical transparency, better insulating and mechanical properties, as well as superior corrosion resistance.

1. Introduction

Aluminum oxide (Al_2O_3) films having excellent optical transparency, insulating and mechanical properties, as well as corrosion resistance are widely used in electronic devices and displays for surface protection [1–7]. However, the properties and performance of Al_2O_3 are intricately related to the crystalline structure and film density. Vapor deposition techniques typically yield amorphous Al_2O_3 [8–10]. Therefore, their density is of vital importance.

Among the common vapor deposition techniques, magnetron sputtering is generally the preferred industrial method to deposit Al_2O_3 films due to the controllability, film uniformity, process stability, and high yield [11–13]. In conventional magnetron sputtering, the density of Al_2O_3 films is mainly regulated by the deposition temperature and particle energy [13–16]. Cloud et al. have elevated the deposition temperature to 480 °C to improve the particle mobility and subsequently, the film density [17]. However, the deposition temperature during magnetron sputtering typically needs to be controlled to be below 400 °C to prevent vacuum sealing issues and malfunction of most functional devices. Moreover, the density of aluminum oxide exhibits minimal variation below 400 °C [18]. The particle energy is the other important parameter in magnetron sputtering. By decreasing the working pressure and target-to-substrate distance, gas-phase collisions can be reduced to increase the particle impact energy [19,20]. However, the intrinsic energy of these particles typically remains below 10 eV, which limits the impact on film densification. Researchers have also sought to enhance the ion ratio and energy by regulating the discharge in order to increase the energy of the deposited particles [21–24]. E. Wallin have utilized high-power impulse magnetron sputtering (HiPIMS) to increase both the ionization rate and energy in the deposition of aluminum oxide and discovered that oxide densification increases with the particle energy [22]. In addition, a high bias voltage further enhances the energy providing another means to tailor the film density. Nonetheless, owing to the insulating nature of aluminum oxide, a high bias leads to the accumulation of electrical charges on the sample surface, which in turn triggers severe arcing leading to film damage.

* Corresponding authors.
E-mail addresses: liull620@163.com (L. Liu), wuzz@pkusz.edu.cn (Z. Wu).
[1] The authors make equal contributions.

https://doi.org/10.1016/j.tsf.2025.140611
Received 15 May 2024; Received in revised form 10 October 2024; Accepted 20 January 2025
Available online 21 January 2025

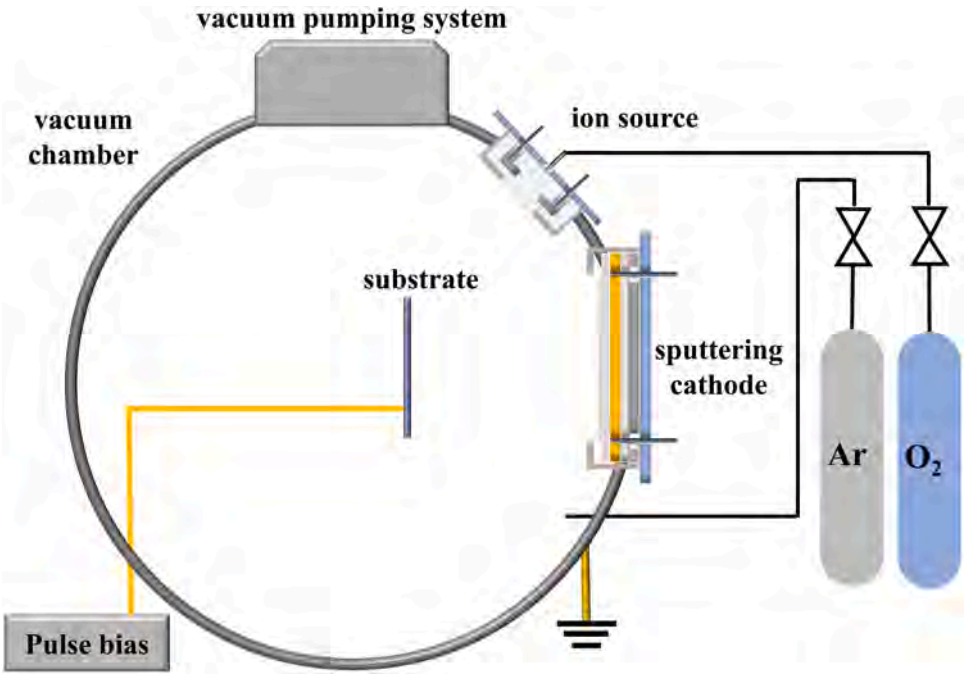

Fig. 1. The schematic picture of the film depositing equipment.

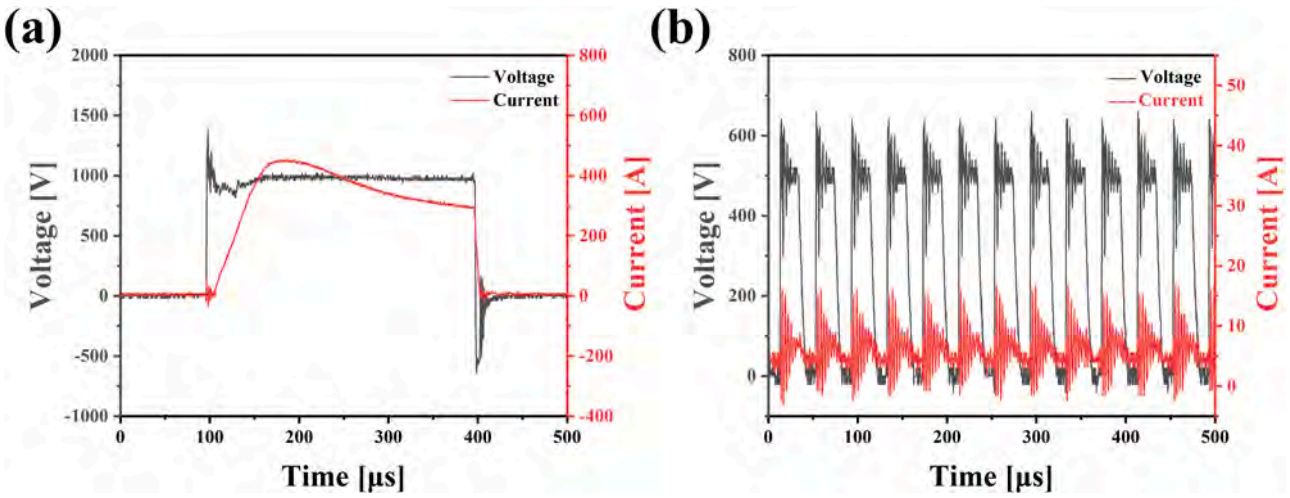

Fig. 2. The discharge waveform of (a) HiPIMS (b) medium-frequency.

Herein, in order to increase the particle energy and ionization rate while suppressing arcing, kV pulsed biasing is adopted in the deposition of Al_2O_3 films by high-power impulse magnetron sputtering (HiPIMS). In this technique, high density Al and O ions with energies on the order of thousands of eV are generated. The effects of biases are studied by systematically analyzing the structure and properties of the deposited Al_2O_3 films. Our results reveal that kV pulsed biasing improves the film density, optical transparency, insulating and tribological properties, as well as corrosion resistance.

2. Experimental details

The substrates were 304 stainless steel pieces (30 × 30 × 1 mm^3) and sodium-calcium glass slides (20 × 20 × 1 mm^3). The substrates were ultrasonically cleaned in anhydrous ethanol for 20 min and dried with compressed air. Before deposition, the vacuum chamber was pumped to a base pressure of 3 × 10^{-3} Pa, and heated to 300 °C to exclude the residual gas contamination. After heating and degassing, the chamber was cooled down to 30 °C, and no additional heating was adopted during film deposition. The schematic of film depositing equipment is shown in Fig. 1.

An aluminum target (99.99 % pure, 390 mm × 160 mm) was used in the vacuum to which a mixture of argon and oxygen was bled for deposition. One ion source((ISP-20S, China Nuclear Tongchuang (Chengdu) Technology Co., Ltd.)) was utilized during substrate cleaning and film deposition processes to generate argon plasma and enhance oxygen ionization. The ion source was working at a power of 300 W. During film deposition, the discharge of aluminum target was triggered at a pressure of 0.5 Pa using argon and oxygen flow rates of 50 sccm and 40 sccm, respectively. Purity of argon and oxygen used for discharging was 99.99 %. The substrate was positioned 40 cm from the target. HiPIMS was carried out with frequency of 50 Hz and pulse width of 300 μs. To enhance the discharge stability, a medium-frequency was superimposed to the HiPIMS pulse. The medium-frequency utilized a

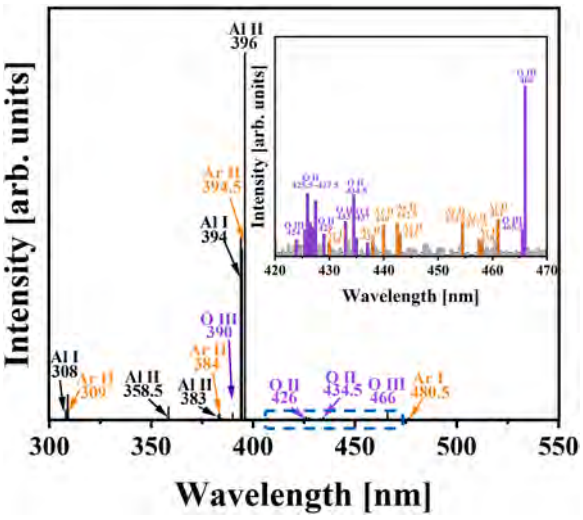

Fig. 3. The plasma emission spectrum near the substrate.

frequency of 25 kHz and pulse width of 20 μs. HiPIMS and medium-frequency waveforms were supplied by MELEC GMBH. Typical wave shape of the HiPIMS and medium-frequency discharge pulse waveforms were shown in Fig. 2. The power settings of HiPIMS and medium-frequency discharge were 2700 W and 400 W, respectively. During deposition, oxygen was introduced from ion source with a power of 3 kW to enhance the ionization of oxygen in the chamber and to improve the ability to form compounds. The ion energy and ion intensity were regulated by the pulsed bias. The pulsed bias (PPS-5000, Plasma technol Technology, Hong Kong) frequency was 500 Hz, and the pulse width was 20 μs. In the experiments, different pulsed voltages of 0 V, −1 kV, −2 kV, and −3 kV were adopted to produce the corresponding samples designated as B-0, B-1000, B-2000, and B-3000, respectively. The deposition time was 1 hour.

The surface and cross-sectional morphology of alumina films were characterized by ZEISS SUPRA 55 field emission scanning electron microscope. Oxford X-Max energy spectrometer was utilized to estimate the composition of films. The optical transmittance of the films was determined on the UV-2450 UV–visible spectrophotometer. The refractive index was obtained at the wavelength 550 nm by M-2000VI ellipsometer. According to the Lorentz-Lorenz equation, the density of alumina films was calculated [21,22]. The surface roughness of the films deposited on glass slides were measured by Bruker Dimension Icon atomic force microscope (AFM). The characterization range of AFM was 5 μm × 5 μm. Unidirectional ball-on-disk tests were operated on glass substrate samples for 2000 cycles using a 4 mm-diameter Si_3N_4 ball as counterpart and 2 N normal force was applied to the friction pairs. The diameter of wear tracks was 10 mm. The morphology of wear tracks was measured by the DEKTAK XT stylus profilometer to calculate the wear rate. The scanned length of profilometer was set to 1000 μm. The surface morphology of the wear track was also examined under a VK-X200 3D laser confocal microscope. Before testing the morphology of the wear tracks, samples are sonicated in anhydrous ethanol for one minute to remove debris. The hardness of the films was evaluated by a micro-hardness tester (Fischerscope-HM2000) using a maximum load of 10 mN.

3. Results and discussion

To investigate the composition of the plasma near the substrate, the plasma spectrum in proximity to the substrate was characterized by spectrometer, as depicted in Fig. 3. The spectrum primarily comprises Ar I (458.0 nm and 480.5 nm), Ar II (309.0 nm, 384.0 nm, 394.5 nm and 480.5 nm), Al I (308 nm), Al II (358.5 nm, 394.5 nm and 396 nm), O I (437.0 nm), O II (426.0 nm and 434.5 nm), and O III (390.0 nm, 465.5

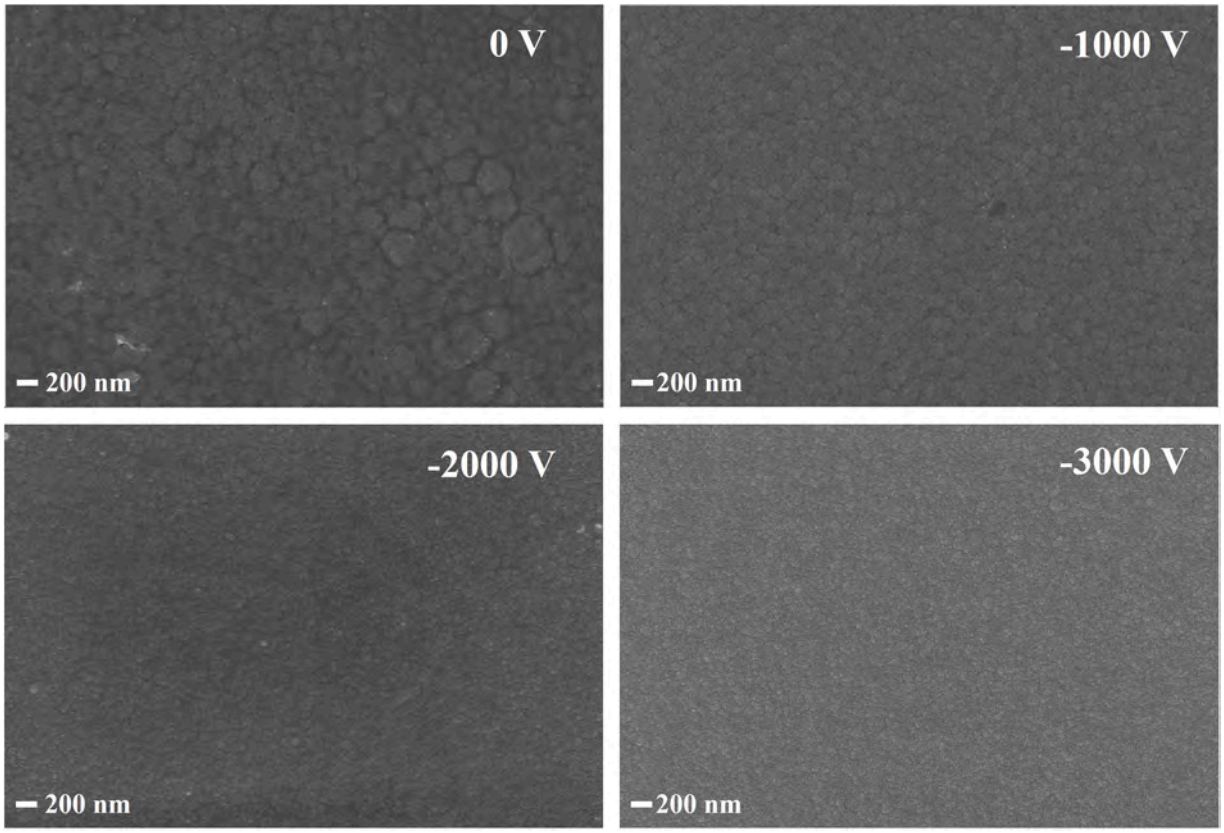

Fig. 4. Surface morphology of different samples.

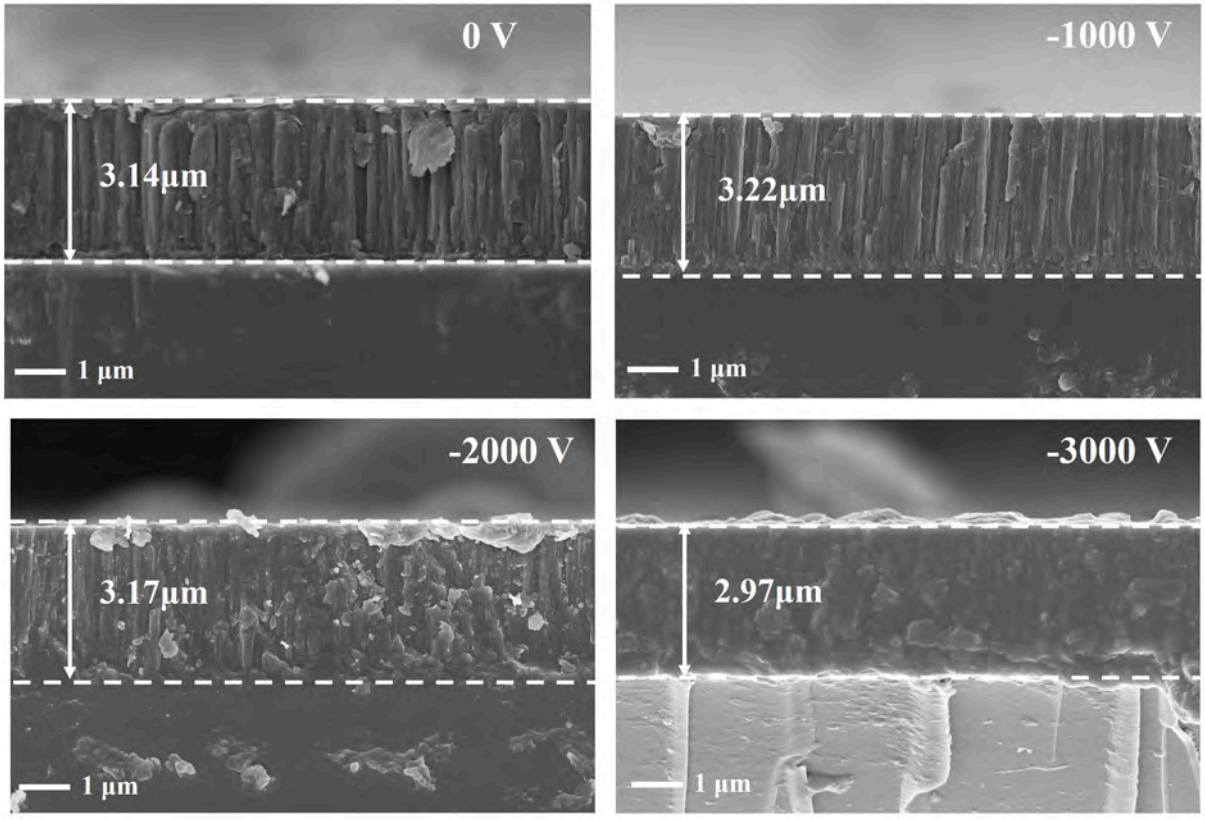

Fig. 5. Cross-sectional morphology of different samples.

nm and 466.0 nm) in HiPIMS discharge. Notably, the peak intensities of ionized species (Al II, O II, and O III) are much higher than those of atomic species (Ar I, O I, Al I) as a result of the high intensity HiPIMS discharge. The highly ionized O and Al ions can be affected by the negative pulse bias voltage, thereby regulating their energy and consequently impacting the quality of the films.

The surface morphology in Fig. 4 does not show obvious pores or defects in all the samples. The clusters in the films prepared without a bias are uneven in size, with some clusters reaching a size of several hundred nanometers. The connections among large and small clusters are loose, indicating a small film density. With increasing biases, the cluster size decreases, and the gaps between them narrow progressively, suggesting that the film density increases. In the absence of a bias, ions generated from the target reach the substrate with low energy, resulting in a loosely stacked film. However, when a negative substrate bias is applied, ions bombard the substrate with a higher energy producing more etching effects [25]. The gaps between clusters are compacted by ion bombardment, while the loose structures are etched leaving denser areas and giving rise to a larger film density. As importantly, even at a high pulsed bias, no arcing is observed inside the vacuum chamber, thus producing fewer defects in the coatings.

According to the cross-sections of the films (Fig. 5), the thicknesses of B-0, B-1000, B-2000, and B-3000 are 3.14 μm, 3.22 μm, 3.17 μm, and 2.97 μm, respectively. The bias voltage attracts ions and potentially increases the deposition rate. However, if the voltage is excessively high, ion etching and larger density can reduce the film thickness. Consequently, with increasing biases, the film thickness rises initially but declines subsequently. B-0 exhibits the typical columnar morphology with significant undulations in the cross-section. Its poor film density correlates with the uneven cluster size. However, when a pulsed bias is applied, the size of the columnar structure decreases (B-1000 and B-2000), and the individual structure becomes less distinct. The columnar structure cannot be observed from B-3000 and the film density increases.

Fig. 6 shows the AFM images (5 μm × 5μm) of alumina films deposited on glass slides. It can be seen that the cluster size gradually decreases with the increase of bias, which is consistent with the results observed by SEM. The calculated roughness was presented in Fig. 7. With higher substrate bias being applied, the average roughness (Ra) of alumina films decreased from 2.29 nm to 1.71 nm, and root-mean-square roughness (Rq) decreased from 2.86 nm to 2.17 nm (as shown in Fig. 7). The bias could improve ion energy resulting in ion bombardment and increased atom mobility on the surface, filling the gaps between clusters. Thus, higher surface flatness of alumina films was achieved when higher substrate bias was applied.

The composition of the films determined by EDS is shown in Fig. 8. Without a bias, the Al/O ratio is 0.69, which is slightly larger than the stoichiometric ratio of Al_2O_3, suggesting oxygen deficiency and the presence of oxygen vacancies. When a pulsed bias is applied, oxygen ions are attracted to the substrate with higher energy for better film formation. Consequently, the oxygen content increases. At a bias of −1 kV, the oxygen content drops below the Al_2O_3 stoichiometric ratio and stabilizes despite further increasing the bias.

The optical properties of the aluminum oxide films prepared at various biases and the calculated films density are presented in Fig. 9. The average transmittance across the visible light spectrum (390 nm-780 nm) shows an increasing trend with biases, changing from 92.6 % for B-0 to 95.5 % for B-3000. The average transmittance stabilizes after a bias voltage of −2 kV. The higher film density reduces light absorption by internal voids and scattering by surface clusters, consequently increasing transmittance. The refractive indexes at 550 nm rise from 1.56 to 1.60. The refractive index of Al_2O_3 films varies in a relatively broad range from 1.50 to 1.80 in the previous articles [21,26–30]. It is higher at higher deposition power, higher depositing temperature and higher oxygen partial pressure [21,26–30]. The higher deposition power and temperature may befit the crystallization, thereby increasing the

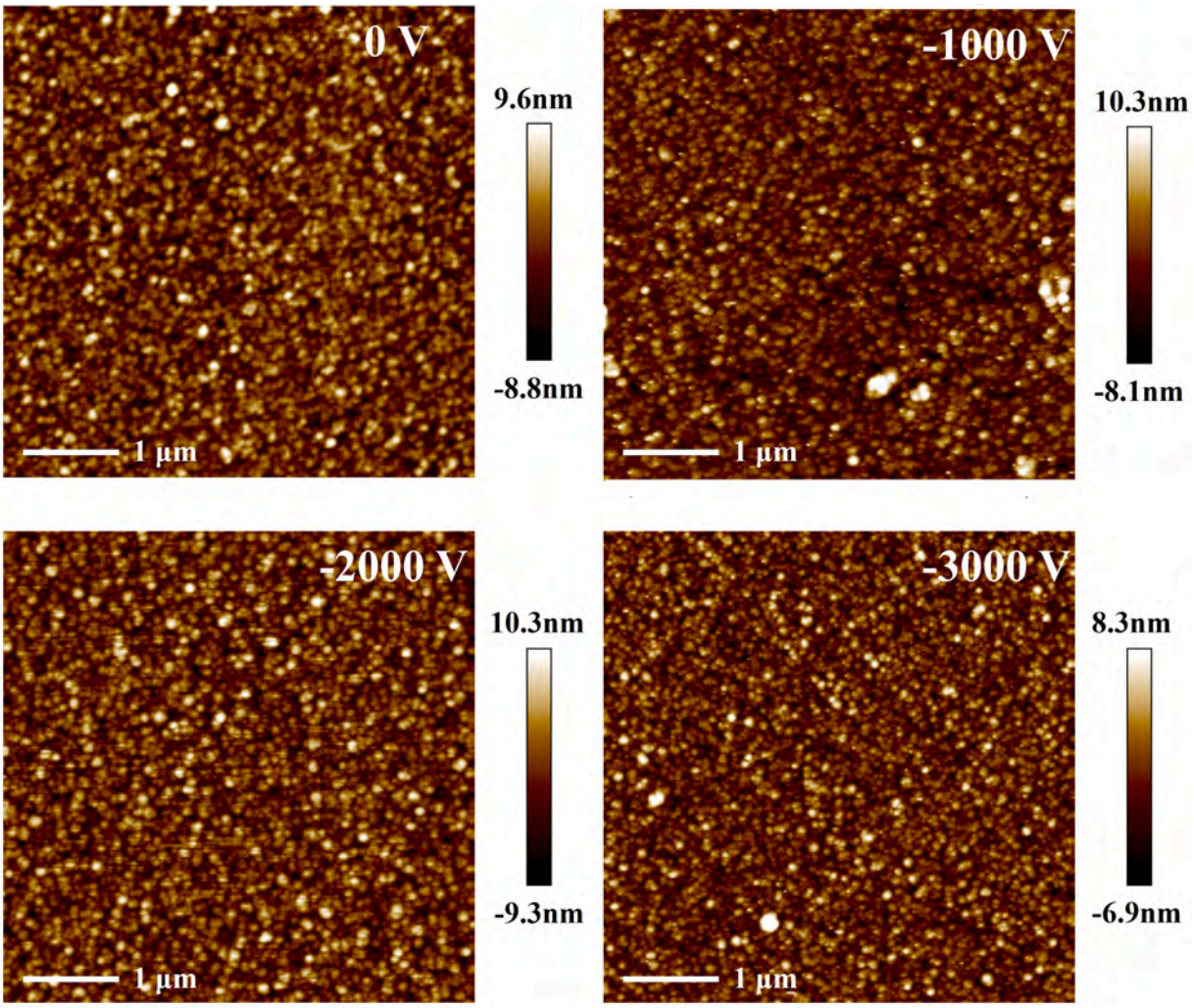

Fig. 6. AFM images of alumina films (image dimensions are 5 μm × 5 μm).

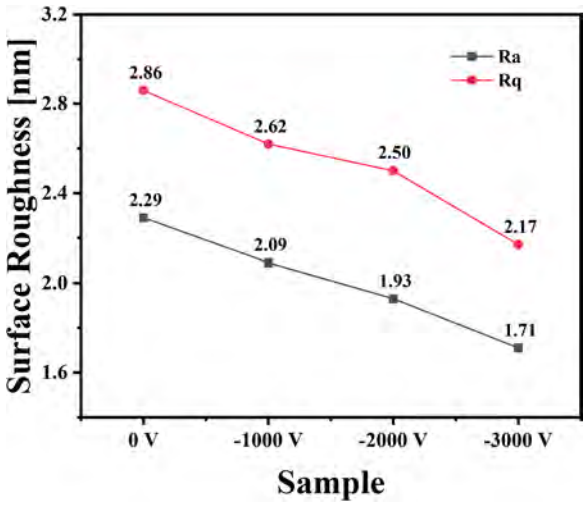

Fig. 7. Surface roughness of different samples.

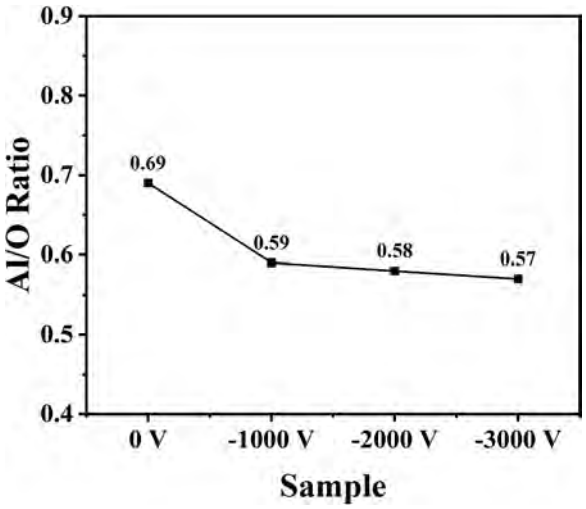

Fig. 8. Al/O ratios for different biases.

refractive index [21,27,28]. Higher oxygen partial pressure may affect the film composition and result in different refractive index [28–30]. In this work, the O content increases with the rising bias, and the refractive index also increase from 1.56 to 1.60. Although it is not high for Al_2O_3 film, it is higher than those reported for HiPIMS method (lower than 1.60) at similar depositing temperature [26]. Higher refractive index always generates from increased film density from 2.91 g/m^3 to 3.08 g/m^3 shown in Fig. 9.

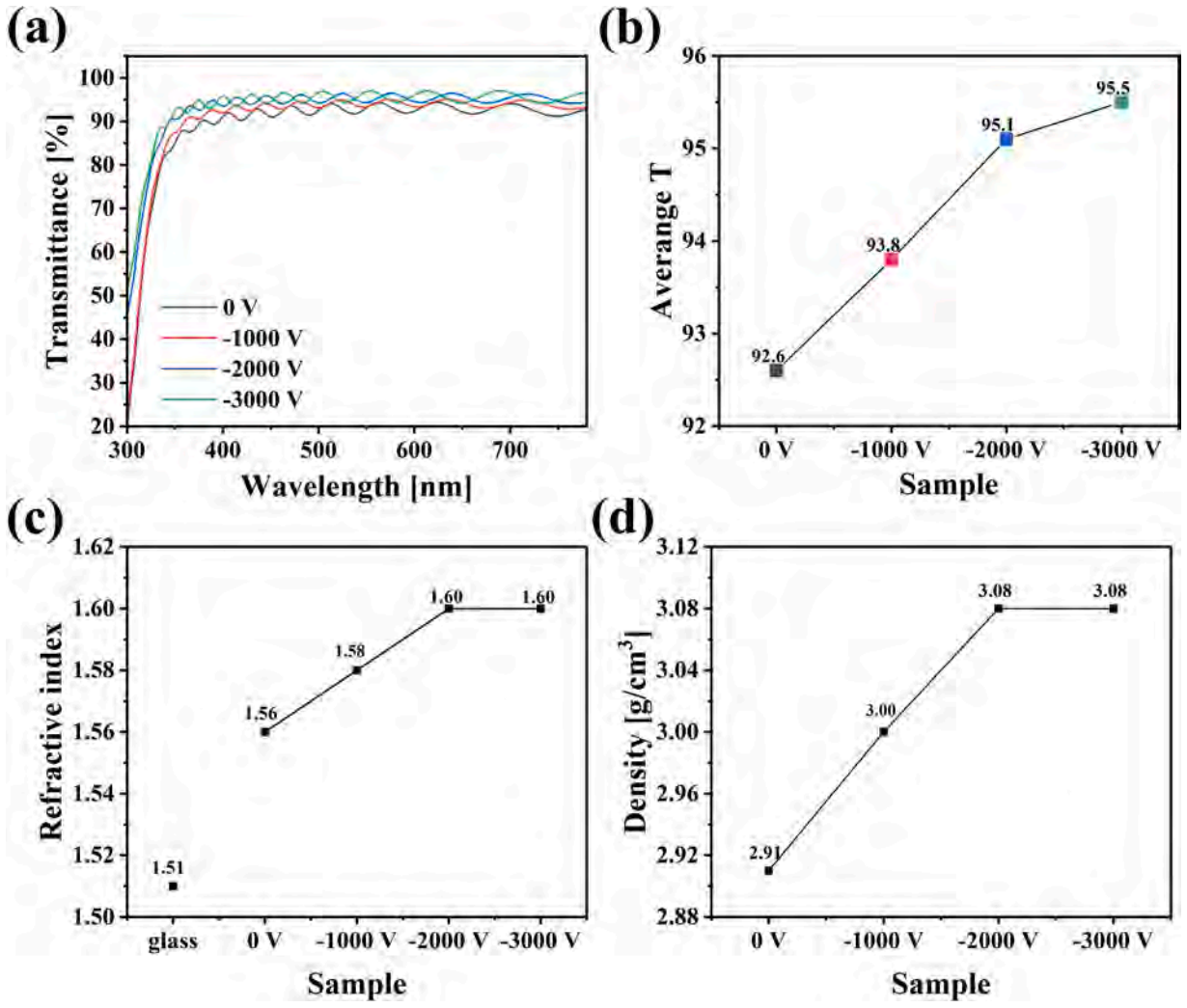

Fig. 9. Optical properties and density of Al_2O_3 films: (a) transmittance (b) average transmittance across the visible light spectrum (390 nm-780 nm) (c) refractive indexes (d) film densities calculated from refractive indexes.

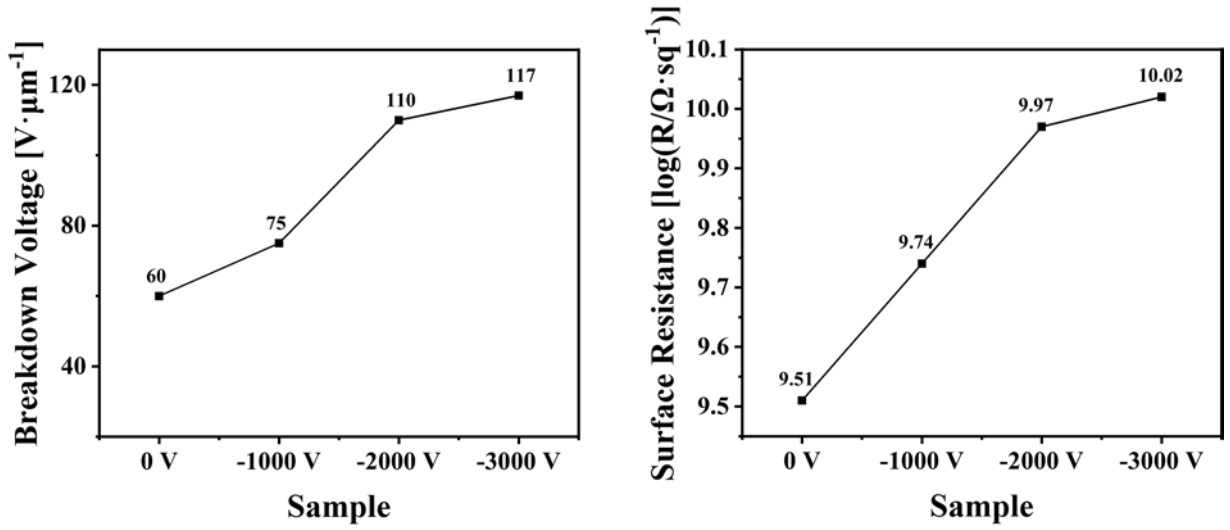

Fig. 10. Insulating properties of Al_2O_3 films: breakdown voltage and surface resistance.

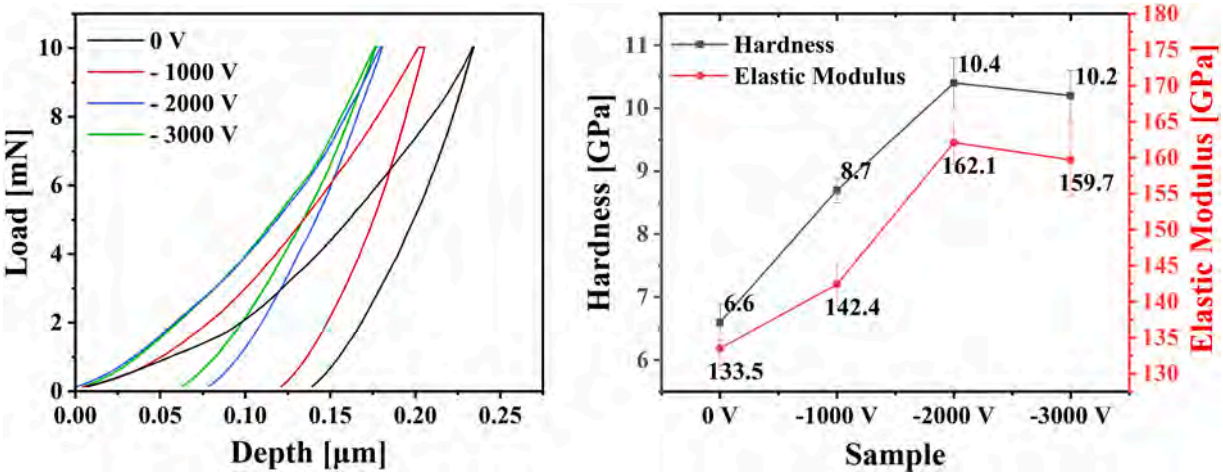

Fig. 11. Mechanical properties of Al_2O_3 films.

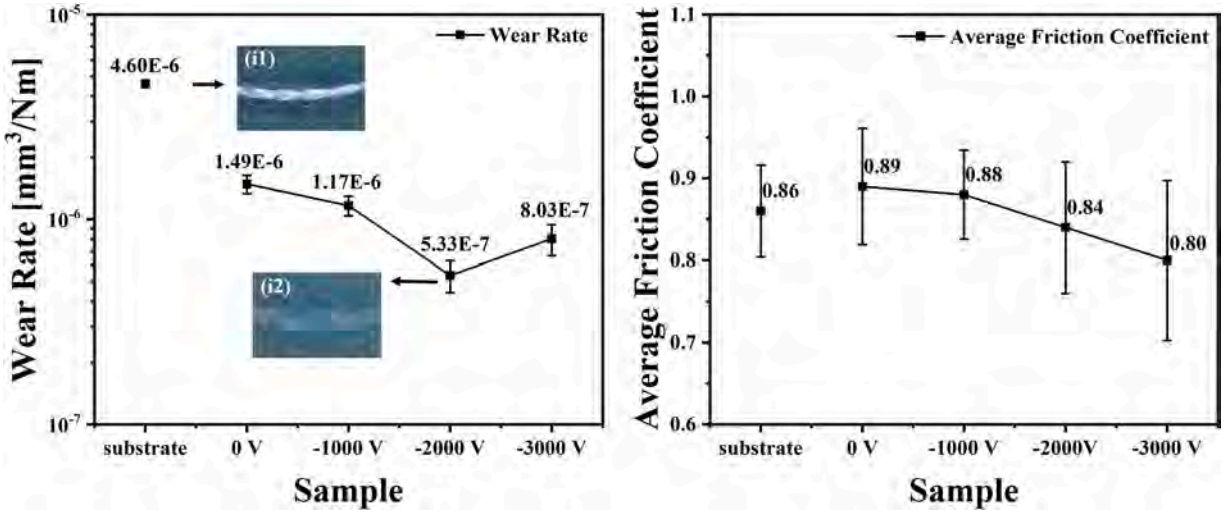

Fig. 12. Wear rates and average friction coefficient of glass substrate and alumina films (i1) image of glass wear track (i2) image of B-2000 wear track.

The electrical properties of the films are shown in Fig. 10. With a bias voltage, the insulating strength of B-0 is only 60 V/μm. This is mainly because the oxygen content is below the stoichiometric ratio. Oxygen vacancies increase the amount of charge carriers and render the film more electrically conductive. By applying pulsed biases, the oxygen concentration increases reaching and exceeding the stoichiometric value eventually, consequently reducing the number of charge carriers and making the films more insulating. Moreover, with increasing pulsed

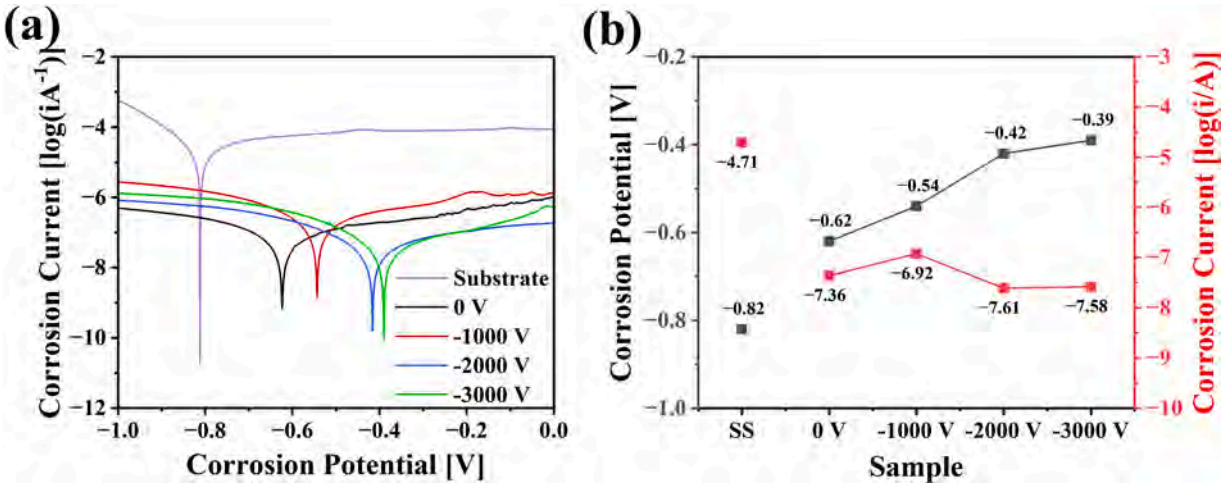

Fig. 13. Corrosion resistance of different samples: (a) Tafel curves and (b) Corrosion potentials and voltages.

biases, the film density also improves, gradually elevating the dielectric strength to 117 V/μm and increasing the surface resistance to $10^{10.02}$ Ω/sq.

The mechanical properties of the Al_2O_3 films are determined by nanoindentation, and the load-displacement curves are presented in Fig. 11. With increasing pulsed biases, the maximum indentation depth decreases gradually from 0.235 μm to 0.177 μm reflecting increasing hardness. The hardness and elastic moduli calculated from the load-displacement curves are presented in Fig. 11. Without a bias voltage, the hardness of the B-0 Al_2O_3 film deposited via HiPIMS is only 6.6 GPa. On the other hand, by applying a bias, the Al_2O_3 films become denser and have enhanced resistance against deformation, leading to a gradual increase in hardness to 8.7 GPa, 10.2 GPa, and 10.4 GPa. Correspondingly, the elastic moduli increase to 133.5 GPa, 142.4 GPa, 159.7 GPa, and 162.4 GPa. The hardness of Al_2O_3 film is mainly related to its crystallinity. Crystalized Al_2O_3 films typically show high hardness over 20 GPa [31]. The hardness of amorphous Al_2O_3 films was mainly affected by film density. The ion bombardment increases film density from 2.91 g/m^3 to 3.08 g/m^3, therefore resulting in higher hardness compared with amorphous Al_2O_3 films in the previous articles (between 7.0~9.0 GPa) [18,32,33].

Ball-on-disk tribological tests are conducted on glass substrate samples and the results are shown in Fig. 12. The brittleness of sodium calcium glass caused crack and severe wear when rubbing with Si_3N_4 ceramic ball. According to the optical images of wear tracks, it can be seen that the alumina films exhibit better toughness and wear resistance compared to the glass substrate. The wear rate of the glass substrate is 4.60×10^{-6} mm^3/N•m. The average friction coefficient of alumina films shows a slightly decreasing trend, which may be attributed to decreasing surface roughness with bias. The wear rate declines drastically especially for the −2000 V sample reaching 5.33×10^{-7} mm^3/N•m which is relatively low compared with the previous reported data (ranging from 1.4×10^{-5} to 5×10^{-7} mm^3/N•m) [34–36]. The low wear rate may be attributed to the dense amorphous structure avoiding the abrasive wear.

To investigate the corrosion resistance of the Al_2O_3 films, Tafel curves are acquired from the films deposited on stainless steel. As shown in Fig. 13(a), with increasing biases, the polarization curves shift gradually toward positive potentials indicative of higher corrosion potentials. Based on the polarization curves, the corrosion potentials and corrosion currents are derived. Fig. 13(b) shows that the corrosion potentials increase gradually from −0.82 V of the substrate to −0.39 V, while the corrosion current diminishes to approximately $10^{-7.6}$. The higher corrosion potential and lower corrosion current confirm better corrosion resistance [37], which is attributed to the higher film density.

4. Conclusion

This study addresses the challenges of controlling the ion energy and film properties encountered during the preparation of Al_2O_3 films by magnetron sputtering. By using kV pulsed bias, the properties of the Al_2O_3 films can be controlled. The pulsed bias enhances the film density and increases the oxygen content in the films. Owing to the dense structure and fully oxidized aluminum atoms, excellent transmittance (95.5 %) and insulating properties are achieved. Moreover, raising the bias voltage increases the film hardness from 6.6 GPa to 10.4 GPa in addition to better wear resistance and corrosion resistance. The results reveal a strategy to produce high-quality films with controlled properties.

CRediT authorship contribution statement

Dongjie Yang: Writing – review & editing, Writing – original draft, Data curation. **Yaoyao Liu:** Supervision, Funding acquisition. **Xiang Zhang:** Data curation. **Shusheng Chen:** Data curation. **Xiaowei Wang:** Resources. **Yu Liao:** Data curation. **Xiaokai An:** Supervision, Investigation. **Yanfei Zhao:** Funding acquisition. **Lingjie Chen:** Funding acquisition. **Suihan Cui:** Writing – original draft, Data curation. **Liangliang Liu:** Writing – review & editing, Writing – original draft, Supervision, Data curation. **Ricky K Y Fu:** Writing – review & editing. **Paul K Chu:** Writing – review & editing, Supervision. **Zhongzhen Wu:** Writing – review & editing, Writing – original draft, Supervision, Project administration, Conceptualization.

Declaration of competing interest

The authors declare that they have no known competing financial interests or personal relationships that could have appeared to influence the work reported in this paper.

Acknowledgments

This work was financially supported by the Shenzhen Science and Technology Research Plan (Grant No. SGDX20201103095406024, KJZD20231023100304009), Sustainable Supporting Funds for Colleges and Universities in 2022 (Grant No. 20220810143642004), National Natural Science Foundation Youth Science Fund project (Grant No. 52305174), Postdoctoral Research Fund Project after Outbound of Shenzhen (Grant No. 6700200201), Shenzhen - Hong Kong Technology Cooperation Funding Scheme (TCFS) (Grant No. GHP/149/20SZ or CityU 9440296), City University of Hong Kong Internal Fund for ITF Projects (Grant No. 9678148), City University of Hong Kong Donation Research Grants (Grant Nos. DON-RMG 9229021 and 9220061), and City University of Hong Kong Strategic Research Grant (SRG) (Grant No. 7005505).

Data availability

Data will be made available on request.

References

[1] J. Szívós, M. Serényi, E. Gergely-Fülöp, T. Lohner, G. Sáfrán, Nanopattern formation in UV laser treated a-AlO_x and nc-Al/AlO_x layers, Vacuum. 109 (2014) 200–205, https://doi.org/10.1016/j.vacuum.2014.07.024.
[2] P. Nayar, A. Khanna, D. Kabiraj, S.R. Abhilash, B.D. Beake, Y. Losset, B. Chen, Structural, optical and mechanical properties of amorphous and crystalline alumina thin films, Thin. Solid. Films. 568 (2014) 19–24, https://doi.org/10.1016/j.tsf.2014.07.053.
[3] P. Schoderböck, On the relationship between texture characteristics and residual stress levels: aan X-ray diffraction study on α-Al_2O_3 hard coatings, Thin. Solid. Films. 777 (2023) 139893, https://doi.org/10.1016/j.tsf.2023.139893.
[4] A. Rajib, K.M. Enamul, S. Kurosu, T. Ukai, M. Tokuda, Y. Fujii, T. Hanajiri, R. Ishikawa, K. Ueno, H. Shirai, Synthesis of AlO_x thin films by atmospheric-pressure mist chemical vapor deposition for surface passivation and electrical insulator layers, J. Vac. Sci. Technol. A 38 (2020) 033413, https://doi.org/10.1116/1.5143273.
[5] M. Li, M. Yao, W. Gao, Z. Su, X. Yao, Self-enhanced electrical performance and less defective electrode/film structure for Al_2O_3 capacitor via interfacial anodic oxidation, Electrochim. Acta 313 (2019) 20–30, https://doi.org/10.1016/j.electacta.2019.04.187.
[6] B.V.T. Hanby, B.W. Stuart, C. Grant, J. Moffat, J. Blissett, C. Gerada, M. Gimeno-Fabra, D.M. Grant, Dielectric breakdown of alumina thin films produced by pulsed direct current magnetron sputtering, Thin. Solid. Films. 662 (2018) 145–154, https://doi.org/10.1016/j.tsf.2018.07.004.
[7] J. Bao, X.-P. Wang, L.-J. Wang, M.-Y. Zhao, J.-Z. Wang, Green electroluminescence of Al_2O_3 film, Vacuum. 201 (2022) 111080, https://doi.org/10.1016/j.vacuum.2022.111080.
[8] C.F. Struller, P.J. Kelly, N.J. Copeland, C.M. Liauw, Characterization studies of aluminum oxide barrier coatings on polymeric substrates, J. Vac. Sci. Technol. A 30 (2012) 023415, https://doi.org/10.1116/1.4709451.
[9] K. Koski, J. Hölsä, P. Juliet, Deposition of aluminium oxide thin films by reactive magnetron sputtering, Surf. Coat. Tech. 116-119 (1999) 716–720, https://doi.org/10.1016/S0257-8972(99)00087-0.
[10] H. Yuan, Q. Li, W. Yan, Y. Zhang, L. Chen, P. Pan, J. Luo, B. Liao, X. Ouyang, A novel and efficient technology of depositing Al_2O_3 film for OLEDs thin film encapsulation, Vacuum. 196 (2022) 110741, https://doi.org/10.1016/j.vacuum.2021.110741.
[11] M. Sinha, M.H. Modi, X-ray reflectivity and photoelectron spectroscopy study of aluminum oxide thin film, in: 61st DAE-Solid State Physics Symposium, 2017 080025, https://doi.org/10.1063/1.4980485.

[12] A.K. Saikumar, S.D. Nehate, K.B. Sundaram, A review of recent developments in aluminum gallium oxide thin films and devices, Crit. Rev. Solid State 47 (2022) 538–569, https://doi.org/10.1080/10408436.2021.1922357.
[13] J.C. Ding, T.F. Zhang, R.S. Mane, K.-H. Kim, M.C. Kang, C.W. Zou, Q.M. Wang, Low-temperature deposition of nanocrystalline Al_2O_3 films by ion source-assisted magnetron sputtering, Vacuum. 149 (2018) 284–290, https://doi.org/10.1016/j.vacuum.2018.01.009.
[14] S. Karlsson, P. Eklund, L. Österlund, J. Birch, S. Ali, Effects of deposition temperature on the mechanical and structural properties of amorphous Al–Si–O thin films prepared by radio frequency magnetron sputtering, Thin. Solid. Films. 787 (2023) 140135, https://doi.org/10.1016/j.tsf.2023.140135.
[15] Y. Yalçın, Ö. Arslan, C. İldeş, E. Çokduygulular, Ç. Çetinkaya, B. Kınacı, Electrical and dielectric properties of RF sputtered nano Al_2O_3 film annealed at 400 °C, J. Mater. Sci. Mater. El. 34 (2023) 1786, https://doi.org/10.1007/s10854-023-11222-y.
[16] G. Zhou, L. Wang, X. Wang, Y. Yu, A. Mutzke, Effect of bias voltage on microstructure and optical properties of Al_2O_3 thin films prepared by twin targets reactive high power impulse magnetron sputtering, Vacuum. 166 (2019) 88–96, https://doi.org/10.1016/j.vacuum.2019.04.060.
[17] A.N. Cloud, S. Canovic, H.H. Abu-Safe, M.H. Gordon, M. Halvarsson, TEM investigation of alpha alumina films deposited at low temperature, Surf. Coat. Tech. 203 (2008) 808–811, https://doi.org/10.1016/j.surfcoat.2008.05.034.
[18] M. Sridharan, M. Sillassen, J. Bøttiger, J. Chevallier, H. Birkedal, Pulsed DC magnetron sputtered Al_2O_3 films and their hardness, Surf. Coat. Tech. 202 (2007) 920–924, https://doi.org/10.1016/j.surfcoat.2007.05.061.
[19] P.J. Kelly, R.D. Arnell, Control of the structure and properties of aluminum oxide coatings deposited by pulsed magnetron sputtering, J. Vac. Sci. Technol. A 17 (1999) 945–953, https://doi.org/10.1116/1.581669.
[20] A. Khanna, D.G. Bhat, A. Harris, B.D. Beake, Structure-property correlations in aluminum oxide thin films grown by reactive AC magnetron sputtering, Surf. Coat. Tech. 201 (2006) 1109–1116, https://doi.org/10.1016/j.surfcoat.2006.01.033.
[21] M.P. Ferreira, D. Martínez-Martínez, J.B. Chemin, P. Choquet, Tuning the characteristics of Al_2O_3 thin films using different pulse configurations: mmid-frequency, high-power impulse magnetron sputtering, and their combination, Surf. Coat. Tech. 466 (2023) 129648, https://doi.org/10.1016/j.surfcoat.2023.129648.
[22] E. Wallin, T.I. Selinder, M. Elfwing, U. Helmersson, Synthesis of α-Al_2O_3 thin films using reactive high-power impulse magnetron sputtering, EPL (Europhysics Letters) 82 (2008) 36002. https://iopscience.iop.org/article/10.1209/0295-5075/82/36002.
[23] M. Aiempanakit, A. Aijaz, D. Lundin, U. Helmersson, T. Kubart, Understanding the discharge current behavior in reactive high power impulse magnetron sputtering of oxides, J. Appl. Phys. 113 (2013) 133302, https://doi.org/10.1063/1.4799199.
[24] E. Wallin, U. Helmersson, Hysteresis-free reactive high power impulse magnetron sputtering, Thin. Solid. Films. 516 (2008) 6398–6401, https://doi.org/10.1016/j.tsf.2007.08.123.
[25] J.-C. Woo, S.-H. Kim, C.-I. Kim, Etch characteristics of TiN/Al_2O_3 thin film by using a Cl_2/Ar adaptive coupled plasma, Vacuum. 86 (2011) 403–408, https://doi.org/10.1016/j.vacuum.2011.08.006.
[26] J. Houska, J. Blazek, J. Rezek, S. Proksova, Overview of optical properties of Al_2O_3 films prepared by various techniques, Thin. Solid. Films. 520 (2012) 5405, https://doi.org/10.1016/j.tsf.2012.03.113.
[27] Prashant Singh, Rajesh Kumar Jha, Rajat Kumar Singh, Babu Ram Singh, Preparation and characterization of Al_2O_3 film deposited by RF sputtering and plasma enhanced atomic layer deposition, J. Vac. Sci. Technol. B 36 (2018) 04G101, https://doi.org/10.1116/1.5023591.
[28] Alexander V. Tumarkin, Dobrynya V. Kolodko, Maksim M. Kharkov, Tatiana V. Stepanova, Andrey V. Kaziev, Nikolay N. Samotaev, Konstantin Yu. Oblov, Preparation of Alumina thin films by Reactive modulated pulsed power magnetron sputtering with millisecond pulses coatings, of Alumina Thin films by reactive modulated pulsed power magnetron sputtering with millisecond pulses, Coatings 14 (1) (2024) 82, https://doi.org/10.3390/coatings14010082.
[29] G. Zhou, L. Wang, X. Wang, Y. Yu, Influence of magnetic field configuration on plasma characteristics and thin film properties in dual magnetron reactive high power impulse magnetron sputtering discharge with Al in Ar/O_2 mixture, Surf. Coat. Tech. 409 (2021) 126837, https://doi.org/10.1016/j.surfcoat.2021.126837.
[30] M. Serényi, T. Lohner, G. Sáfrán, J. Szívós, Comparison in formation, optical properties and applicability of DC magnetron and RF sputtered aluminum oxide films, Vacuum. 128 (2016) 213–218, https://doi.org/10.1016/j.vacuum.2016.03.033.
[31] T. Kohara, H. Tamagaki, Y. Ikari, H. Fujii, Deposition of α-Al_2O_3 hard coatings by reactive magnetron sputtering, Surf. Coat. Technol. 185 (2004) 166–171, https://doi.org/10.1016/j.surfcoat.2003.11.017.
[32] J.C. Ding, T.F. Zhang, R.S. Mane, K.-H. Kim, M.C. Kang, C.W. Zou, Q.M. Wang, Low-temperature deposition of nanocrystalline Al2O3films by ion source-assisted magnetron sputtering, Vacuum. 149 (2018) 284–290, https://doi.org/10.1016/j.vacuum.2018.01.009.
[33] X. Yin, X. Li, H. Wang, K. Zhao, J. Wang, L. Chen, Z. Wu, Y. Chen, The corrosion behavior of Al/Al_2O_3 composite films with ultra-dense structure exposed to lead-bismuth eutectic at 450 to 650 °C, Coatings 13 (2023) 1274, https://doi.org/10.3390/coatings13071274.
[34] R. Westergård, N. Axén, U. Wiklund, S. Hogmark, An evaluation of plasma sprayed ceramic coatings by erosion, abrasion and bend testing, Wear. 246 (2000) 12–19, https://doi.org/10.1016/S0043-1648(00)00506-8.
[35] Z. Hsain, G. Zeng, C.N. Strandwitz, Brandon A. Krick, Wear behavior of annealed atomic layer deposited alumina, Wear. 372-373 (2017) 139–144, https://doi.org/10.1016/j.wear.2016.12.011.
[36] M. Fallqvist, M. Olsson, S. Ruppi, Abrasive wear of texture-controlled CVD α-Al_2O_3 coatings, Surf. Coat. Technol. 202 (2007) 837–843, https://doi.org/10.1016/j.surfcoat.2007.06.063.
[37] M.L. Zheludkevich, I.M. Salvado, M.G.S. Ferreira, Sol–gel coatings for corrosion protection of metals, J. Mater. Chem. 15 (2005) 5099–5111, https://doi.org/10.1039/B419153F.